



# Moment magnitude estimation using Iran strong motion data

Attieh Eshaghi · Abdelkrim Aoudia ·  
Mohammad P. Shahvar · Esmail Farzanegan

Received: 5 March 2022 / Accepted: 3 August 2022 / Published online: 15 August 2022  
© The Author(s), under exclusive licence to Springer Nature B.V. 2022

**Abstract** In this study, seismic moment, moment magnitude, and the corner frequency of Iranian earthquakes were estimated using the Iran Strong Motion Network (ISMN) data. To estimate the source parameters, Andrews (1986) method in frequency domain is employed. In this study, two horizontal components of

the recordings were processed, filtered, and corrected for geometrical spreading and intrinsic attenuation and then have been used in source spectrum calculation. Here, two time windows were selected (1: S-wave and 2: from P- to end of S- window) and the results show that both windows provide acceptable results with similar mean residuals and standard deviations. However, the smallest standard deviation is related to S-window. In total, the moment magnitude for about 4171 records have been calculated. We validated our results for 209 earthquakes with at least three recorded accelerograms that had available reported moment magnitude. The results indicated that the estimated magnitudes are in good accordance with the reported moment magnitudes with mean residual of about 0.07 and standard deviation of about 0.2. This method can be employed in real time or near real time procedure, where both seismic moment and moment magnitude can be calculated soon after the earthquake originated just using available strong motion data. This information would be very helpful in crisis management so that more effective emergency response and recovery plan can be provided in future earthquakes.

## Highlights

- 1- Earthquake source parameters including seismic moment, moment magnitude, and the corner frequency were estimated for Iranian earthquakes using strong motion data. A large database of accelerograms (more than 4000) recorded by Iran Strong Motion Network has been used.
- 2- Andrews's method that is based on Brune source model is used in frequency domain to calculate the moment magnitude. Two time windows were selected to be used in the analysis and the results were validated for 209 earthquakes that had reported moment magnitude. Results show good agreement between calculated and reported magnitudes for both selected windows.
- 3- The results suggest the use of this method and strong motion data for moment magnitude calculation for earthquakes that have not reported moment magnitudes. Also, the outcome of the implementation of this method in real time or near real time would be very helpful in crisis management after earthquake occurrences.

A. Eshaghi (✉) · M. P. Shahvar · E. Farzanegan  
Road, Housing and Urban Development Research Center,  
Tehran, Iran  
e-mail: a.eshaghi@bhrc.ac.ir; attieh.eshaghi@gmail.com

M. P. Shahvar  
e-mail: m.shahvar@bhrc.ac.ir; mshahvar@gmail.com

E. Farzanegan  
e-mail: farzanegan@bhrc.ac.ir; esi.farzanegan@gmail.com

**Keywords** Moment magnitude · Accelerograms ·  
Brune source model · Seismic moment

A. Aoudia  
SISSA-Room 222- Abdus Salam International Centre  
for Theoretical Physics, Earth System Physics, Trieste,  
Italy  
e-mail: aoudia@ictp.it

## 1 Introduction

Generally, earthquake magnitude scales were defined due to the necessity for an objective measure of an earthquake's size. The general concept of earthquake magnitude was introduced by Richter in the early 1930s as a quantitative method to measure the strength of earthquakes (Richter 1935). Nowadays, several magnitude scales are common such as local magnitude ( $M_L$ ,  $M_n$  ...), body-wave magnitude ( $m_b$ ), and surface-wave magnitude ( $M_s$ ) (see Kanamori 1983). These scales are dependent on the amplitude and frequency of the recorded seismic waves. These scales can be calculated based on the empirical equations considering the amplitude of the recorded seismic waves; however, they all have a limitation, they become saturated above a certain size. In order to solve this problem, another scale was introduced as the moment magnitude  $M$  or  $M_w$  (Aki 1972; Hanks and Kanamori 1979). This scale is estimated from the seismic moment,  $M_0$ , which is a physical quantity related to the total released energy during an earthquake. The seismic moment can be estimated using different approaches; for instance, it can be calculated in the field based on the measurement of the fault length and the average dislocation, the moment tensor inversion, full waveforms inversion, or using the seismic wave's amplitude spectra (Brune 1970, 1971; Aki and Richards 1980; Boatwright 1980; Abercrombie 1995; Kikuchi and Kanamori 1991). Among these methods, the spectral method is generally based on the Brune source model (Brune, 1970, 1971), where the  $M_0$  is estimated from the low-frequency plateau of the displacement source spectrum that is a simple, yet very efficient method. Some studies (e.g., Abercrombie, 1995; Parolai et al. 2007; Edward et al. 2010; Caprio et al. 2011) used spectral fitting methods to compute the seismic moment. Another studies used a method proposed by Andrews (1986), which is similar to Brune's method and can be used in both time and frequency domain, to estimate the seismic moment (such as Hwang et al. 2001; Shoja-Taheri et al. 2007; Gallo et al. 2014). For instance, Gallo et al (2014) used this method to provide near real-time moment magnitude for earthquakes in Italy, where this procedure has been implemented and routinely provides the magnitude and corner frequency of the earthquakes to Civil Defense. In

the study by Shoja-Taheri et al. (2007), the  $M$  of the Iran earthquakes was calculated based on Andrews' (1986) method in time domain using the Iran Strong Motion Network (ISMN) data. Now, after more than a decade, we have a much better catalogue (in terms of the number of the records, magnitude, and distance).

In this research,  $M_0$ ,  $M$  and the first estimate of the corner frequency ( $f_c$ ) were estimated based on Andrews' (1986) method in frequency domain using Iran strong motion data. The above mentioned source parameters were estimated using two-time spans: the S-wave window (hereafter called S-window) and the window from the first P-arrival up to the end of the S-wave (hereafter called W-window). The results are calculated and presented for all data with good quality. We used this method for strong motion data available at ISMN databank with  $M \geq 3.0$  (see Data and Resources). ISMN is in charge of the operating and management of the Iran Strong Motion Network (Shahvar et al. 2021). Currently, it consists of about 870 three-component Kinematics SSA-2 accelerometers, which are working offline, and just recently, it managed to purchase 700 new modern high-quality three-component Fortis sensors and Minimus digitizers manufactured by Güralp Systems Ltd. with sensor dynamic range of 160 dB and sampling rate of 200 that can provide real time data (Shahvar et al. 2021). Up to date of this manuscript, 500 instruments have been installed and others are in progress to be installed. For more information about the network, acquisition system, transfer, and pre-processing of the data please see Shahvar et al. (2021).

After installation of these new accelerometers, ISMN will be able to implement the proposed method of magnitude estimation on near real-time basis and estimate the moment magnitude rapidly after the earthquake occurrences, which is essential for earthquake early warning and rapid response operations. In addition, the real-time data will provide the earthquake strong motion parameters such as the earthquake waveforms, epicenter location, Fourier and response spectra, peak ground motion parameters, or other related earthquake engineering parameters. This information is crucial in fast evaluation of the earthquake characteristics and its effects and eventually will be used in crisis management, so that more effective emergency response and recovery plan can be provided in future earthquakes.

## 2 Data

In this study, the earthquakes that have been recorded by ISMN stations across the country were used. First, all strong motion data available in the ISMN data bank from March 6, 1977, to April 19, 2018 (Table 1) were selected for earthquakes with  $M > 3.0$  and epicentral distance ( $R$ ) less than 150 km (see Data and Resources). In this stage, 5035 three-component accelerograms were collected. Figure 1 shows the geographic representation of the selected earthquakes along with their recording stations. Figure 2 illustrates the distribution of  $M$  against epicentral distance and focal depth for the selected data. For the records shown in Fig. 2, if reported  $M$  was not available we used the magnitude conversion equations of Shahvar et al. (2013) to calculate the moment magnitude for that event. Most of the collected data were recorded by SSA-2 digital instruments. The accelerograms with good quality, sufficient pre-events (at least 5 s data), and clear P-wave arrival were selected and used in the calculation of the magnitudes.

It is worth mentioning that for earthquakes used in the analysis part, based on the reliable published catalogs (Global Centroid Moment Tensor (CMT), National Earthquake Information Center (NEIC), Iranian Seismological Center (IRSC) and the Shahvar et al. (2013) catalog, respectively), the reported moment magnitudes ( $M_{rep}$ ) for each earthquake were extracted and finally, according to these values, statistical analysis has been carried out. Note that the  $M_{rep}$  are the ones that were reported by reputable agencies. At the end, 1625 accelerograms had the reported moment magnitudes, which have been used in the final evaluations.

**Table 1** Information of the data used in this study

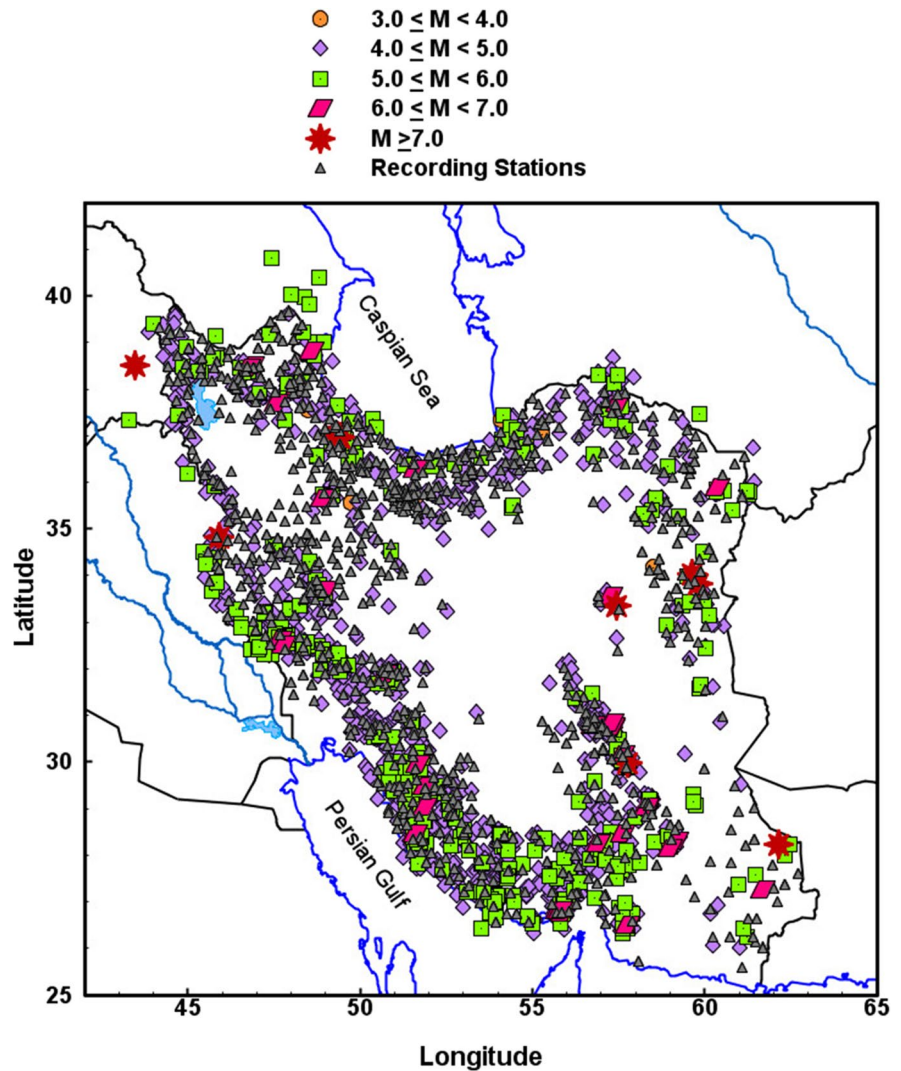
Date	March 6, 1977, to April 19, 2018
Number of accelerograms	5035
Magnitude range	$3.0 \leq M \leq 7.8$
Epicentral distance	0.2–150 km
Depth	$h < 104$ km

## 3 Data processing

To process the data, all accelerograms were first visually inspected, and then, the P- and S- wave's arrivals were determined. During the visual inspection of the data, all accelerograms with very low quality, those that lacked the clear P-wave arrival (either the P-wave was not recorded at all or could not be detected) or the ones that missed one component or contained several S-wave windows (considered as complex events) were ruled out from the database. At the end, 4171 three components accelerograms were collected and were included in the magnitude calculations. To choose the S-wave window, the duration from S-wave arrival to the point that covers the 95% of the accumulated energy of the acceleration record is selected (Bommer and Pereira 1999). Figure 3 shows the three component records of different earthquakes along with the first P and S- arrival and the selected S-window.

In order to calculate the magnitude, accelerograms that had both clear P- and S-wave arrivals and sufficient pre-event signal, which is needed to calculate the signal to noise ratio (SNR), were selected. The duration of noise window is selected from the beginning of the trace and continues until 0.1 s before the first P-arrival. The signal is chosen from the P-arrival to the end of S-wave window (Fig. 3). To choose the usable frequency window in the analysis, we considered the frequency bandwidth where the SNR is larger than 3. The following procedure is applied to the considered frequency range (depending on the signal window, it varies between 0.05 and 50 Hz). First, the range is selected, and then, in the selected range of frequency, SNR is calculated. We checked the obtained SNR values and we chose the window where the obtained SNR is continuously greater than 3. The upper and lower limits of the band-pass filter are also being selected based on the obtained values, where  $f_{low}$  and the  $f_{high}$  are the first frequency and last frequency where we have  $SNR > 3$  respectively (Fig. 4). It should be noted that the data were first base line corrected, windowed, tapered, and then band-pass filtered, and eventually, the corrected acceleration, velocity, and displacement time series were obtained by integration. Then, in order to get the signal spectra, the fast Fourier transform (FFT) was applied. Figure 4 illustrates examples of three components signal and noise spectra recorded from different earthquakes.

**Fig. 1** Geographical distribution of the selected earthquakes in this study (the magnitude range is shown by different symbols) and the recording stations (triangles, operated by ISMN)



#### 4 Calculation of moment magnitude

As it was explained, the moment magnitude scale is related to the seismic moment or  $M_0$ , the physical quantity that is a measure of seismic energy that was introduced about a decade ago by Aki (1966). The unique feature of this scale is that it does not saturate at large magnitudes and expresses the real energy of large earthquakes. Moment magnitude or  $M$  can be estimated using the following equation (Hanks and Kanamori 1979; Aki 1972; Kanamori 1977, 1978):

$$M = 2/3(\log_{10}(M_0) - 9.1), \quad (1)$$

where  $M_0$  is the scalar seismic moment in N.m. In this research, the seismic moment is calculated from Eq. (2) using the low-frequency plateau in displacement spectra ( $\Omega_0$ ).

$$M_0 = \frac{4\pi\rho\beta^3}{U_{\theta\varphi}FPG(R)}\Omega_0, \quad (2)$$

where  $\rho$  is the density ( $2800 \text{ kg/m}^3$ ),  $\beta$  is the shear wave velocity ( $3500 \text{ m/s}$ ), and  $\Omega_0$  is the value of the spectral low frequencies plateau (in  $\text{m/Hz}$ ).  $U_{\theta\varphi}$  is the mean radiation pattern (0.55, Aki and Richards 1980; Boore and Boatwright 1984; Gallo et al. 2014),  $F$  is the free surface amplification (2), and  $P$  is the coefficient of energy partition between two horizontal components

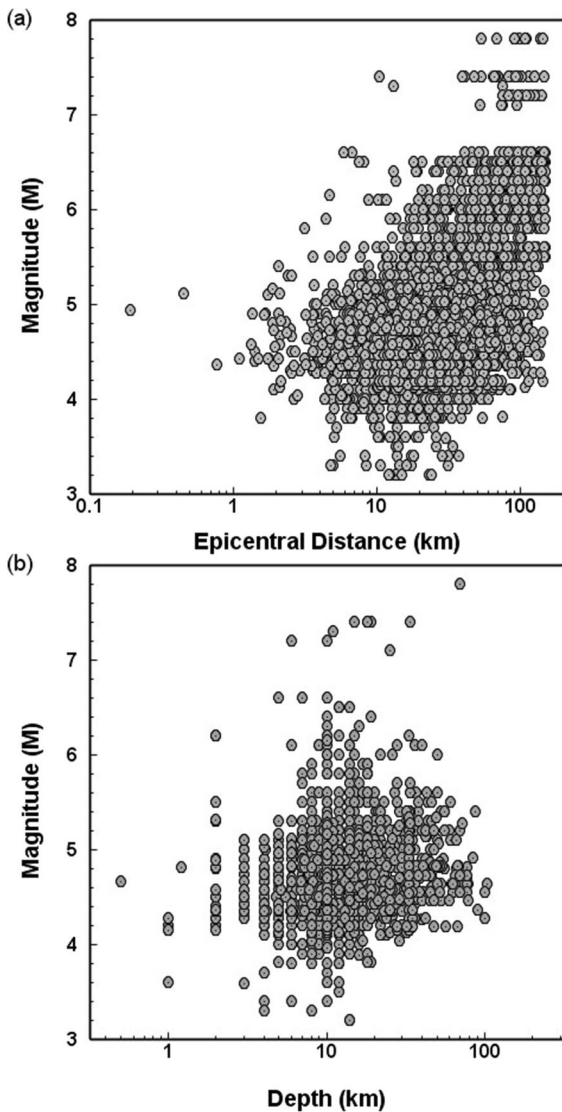


**Fig. 2** Magnitude versus **a** epicentral distance and **b** depth for the data used in this study

(0.7) (Boore, 1983).  $G(R)$  is the geometrical spreading function that represents the decrease in amplitude of the seismic waves because of the geometrical attenuation and is defined using the following equation for the hypocentral distance ( $R$ ) (Davatgari et al. 2021):

$$G(R) = \begin{cases} \left(\frac{1}{R}\right)^{1.01} & R < 70\text{km} \\ \left(\frac{1}{70}\right)^{1.01} \left(\frac{70}{R}\right)^{1.37} & 70 \leq R \leq 150\text{km} \end{cases}, \quad (3)$$

After determining of seismic moment from Eq. (2), the moment magnitude can be estimated from Eq. (1). To calculate  $M$ , different time spans (including the S-wave window and the whole trace record) can be determined and based on the selected window, the magnitude is computed. For example, Shoja Taheri et al. (2007) used different windows and concluded that the use of the S-wave window had the lowest standard deviation, but the use of the whole record that proceeds from the P-wave arrival to the end of the record is simpler, more functional, and offers good results. In this study, magnitudes are calculated using the S-window as well as the W-window (from P- to end of S-wave window). The final seismic moment is determined based on the geometric mean of seismic moments obtained from each strong motion station and based on this final average, the final moment magnitudes are determined, reported and compared.

### 5 Spectral analysis in the Andrews Method (1986)

In Andrews (1986) method, the low-frequency spectrum level ( $\Omega_0$ ) is calculated as follows:

$$\Omega_0 = 2I_D^{3/4} I_V^{-1/4}, \quad (4)$$

where  $I_v$  and  $I_D$  are calculated from the following relationships:

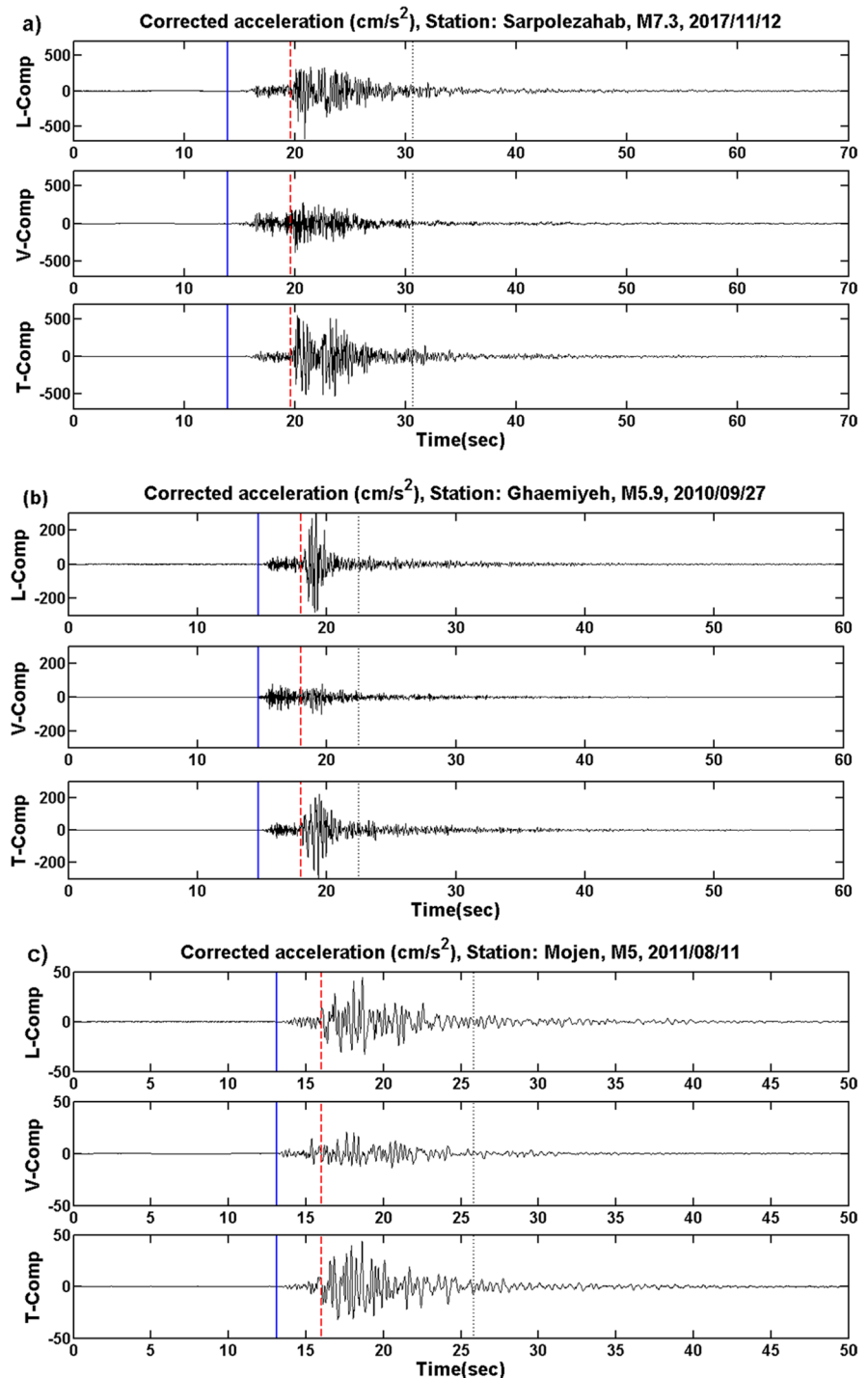
$$I_V = 2 \int_0^{+\infty} V^2(f)df, \quad (5)$$

$$I_D = 2 \int_0^{+\infty} D^2(f)df, \quad (6)$$

In Eqs. (5) and (6),  $V$  and  $D$  are velocities and displacements Fourier spectrum respectively, which, as previously mentioned, are obtained by integrating the accelerograms. The lower and upper limits of the integrals in Eqs. (5) and (6) are from zero to infinity, while the spectrum is practically calculated for a bounded frequency range. Di Bona and Rovelli (1988) have studied and discussed this frequency limitation. They reported that the frequency range in which two integrals must be calculated are limited by two frequencies: first one is the low-frequency cutoff, which is due to the limited time of the strong ground motion, and the second one is



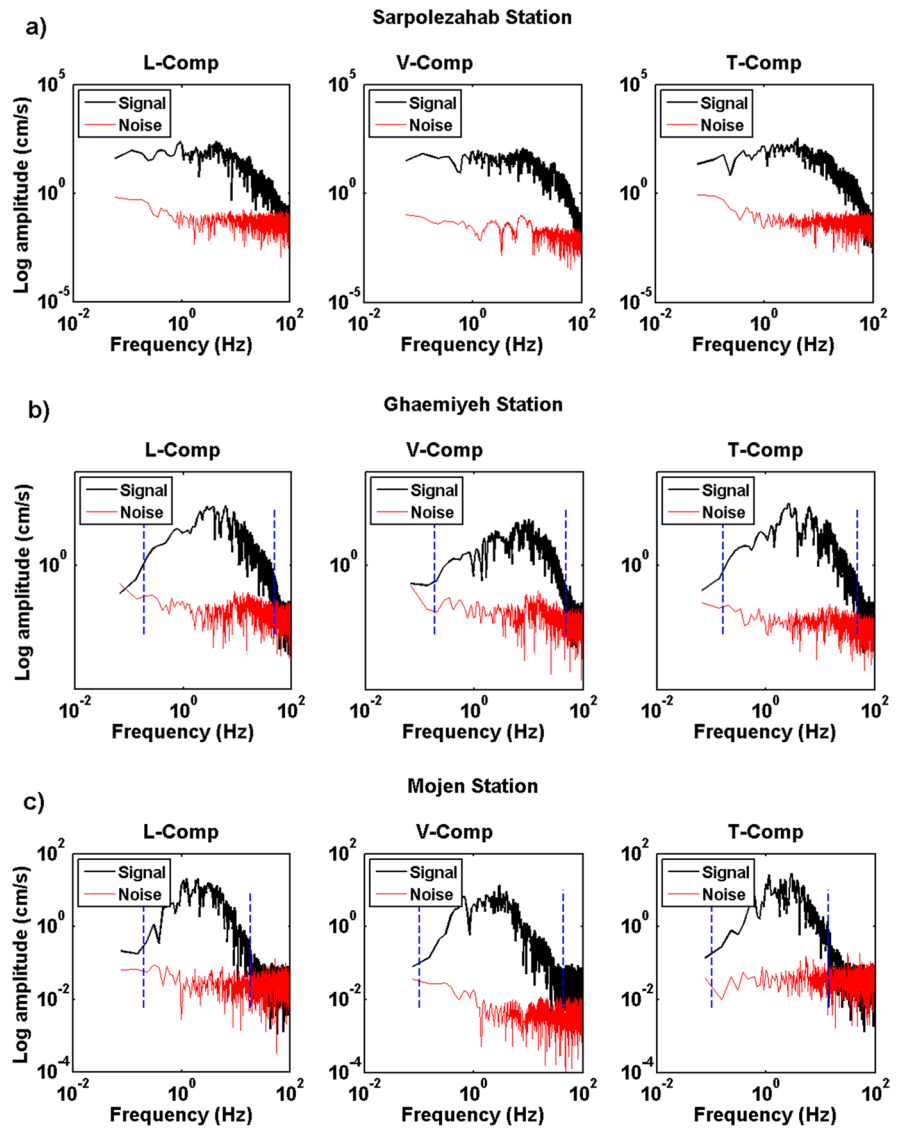
**Fig. 3** Three components of acceleration time series at three stations: **a** 2017 M7.3 Sarpol-e Zahab earthquake at Sarpol-e Zahab station; **b** 2010/09/27, M5.9 event at Gaemiyeh station; and **c** 2011/08/11, M 5.0 event at Mojen station. The P- and S- arrivals are shown with solid and dashed lines respectively. Vertical dotted lines represent the extent of the signal window. L, V, and T represent the North–South, East–West, and vertical component respectively



the high-frequency cutoff, which is determined by the Nyquist frequency. In practice, the usable band is controlled by the instrument's response and the amount of

noise at low and high frequencies (Gallo et al. 2014). Therefore, the two integrals (5) and (6) transform to the following relations:

**Fig. 4** Examples of the three components of the signal and noise spectra at three stations: **a** 2017 M7.3 Sarpol-e Zahab earthquake, recorded at the Sarpol-e Zahab, where excellent SNR in all frequency range is observed and resulted  $f_c = 0.12$  Hz; **b** 2010/09/27, M5.9 event at Gaemiyeh station, and resulted  $f_c = 0.54$  Hz; and **c** 2011/08/11, M 5.0 event at Mojen station and resulted  $f_c = 0.94$  Hz. The  $f_{low}$  and  $f_{high}$  for each component are shown with vertical blue dashed lines



$$I_V = 2 \int_{f_{low}}^{f_{high}} V^2(f)df, \tag{7}$$

$$f_c = \frac{1}{2\pi} \sqrt{\frac{I_V}{I_D}} \tag{9}$$

$$I_D = 2 \int_{f_{low}}^{f_{high}} D^2(f)df, \tag{8}$$

Also, the corner frequency is calculated from these integrals as follows:

It should be noted that in this method, before calculating the magnitudes, the accelerograms are corrected assuming the Davatgari et al. relation (2021) for the inelastic attenuation effect.

$$Q(f) = 146^{0.91}, \tag{10}$$

where  $f$  is the frequency and  $Q(f)$  represents the frequency-dependent attenuation factor (Gallo, et al. 2014; Davatgari et al. 2021).

## 6 Results and validation

In this research, using the recorded accelerograms of the earthquakes in Iran, available at the ISMN's data bank,  $M_0$ ,  $M$  and  $f_c$ , were calculated for each accelerogram. For example, the calculated values of  $M$ ,  $M_0$ , and  $f_c$  at each station for the  $M7.3$  Sarpol-e Zahab earthquake on 2017/11/12, for data with epicentral distance less than 150 km, is shown in Tables 2 and 3 using the S- and W-windows respectively. As it can be seen, the resulted  $M$  values are about 7.1 which are about 0.2 smaller than the reported moment magnitude.

Subsequently, earthquakes with the reported moment magnitude by reputable agencies were separated and the residuals are calculated as the differences between the values obtained in this project ( $M_{cal}$ ) and the reported magnitude ( $M_{rep}$ ) for each accelerogram. Based on the obtained residual values, the mean (Mean) and standard deviation ( $\sigma$ ) of residuals were also calculated that are presented in Table 4. Also, part (a) in Figs. 5 and 6 illustrates the distribution of the magnitude residuals for each record ( $M_{rep}-M_{cal}$ ) versus epicentral distance for the selected windows. The bin-averaged residuals are also shown with squares in the figures, which indicates that in larger distance we have underestimation of the magnitude. Also, it can be seen that the largest underestimation is for the records with larger magnitude as well (i.e.,  $M > 7.0$ ). Part (c) in Figs. 5 and 6 shows the magnitude residuals for each record versus the reported magnitude. Different symbols represent the epicentral range. Again, it can be seen that for larger distances we have more underestimation of the magnitudes. Also for records with  $M < 5$  and epicentral distance  $< 50$  km, we observe more overestimations. Part (d) in Figs. 5 and 6 illustrate the comparison between the resulted magnitude from each record and the reported  $M$  along with its obtained  $\sigma$  (0.35 for W-window and 0.31 for S-window). Note that these observations are related to magnitude of each record that had the reported magnitude.

After this step, the final moment for each earthquake was calculated by geometric averaging of the

**Table 2** The resulted values of seismic moment ( $M_0$ ), estimated magnitude ( $M_{cal}$ ), and corner frequency ( $f_c$ ) for 2017 Sarpol-e Zahab earthquake using accelerograms with epicentral distance less than 150 km based on S-wave window

Record	Station	Epicentral distance (km)	Mcal	M0 (N.m)	fc (Hz)
7384–1	Sarpoleza-hab	39.22	7.22	7.64E+19	0.12
7297	Nosood	47.28	6.81	1.87E+19	0.12
7377–1	Goorsefid	66.1	7.27	8.93E+19	0.09
7302–1	Kerend	66.33	7.36	1.22E+20	0.13
7310	Degaga	67.31	7	3.50E+19	0.12
7279	Palangan	69.5	6.99	3.41E+19	0.12
7290	Sarv Abad	69.63	6.9	2.51E+19	0.14
7287	Marivan	82.54	6.86	2.19E+19	0.16
7317	Shoeisheh	92.65	7.01	3.73E+19	0.1
7278	Kamyaran	92.97	6.92	2.71E+19	0.16
7313	Eslama-badqarb	96.33	7.49	1.90E+20	0.15
7295	Mahidasht	101.45	7.04	4.01E+19	0.26
7281	Sanandaj2	113.33	6.83	1.95E+19	0.15
7280	Sanandaj1	113.59	7.05	4.17E+19	0.1
7294	Homail	124.91	7.6	2.84E+20	0.09
7311	Deh Golan	146.44	7.07	4.58E+19	0.16
Mean			7.1	4.81E+19	0.14

seismic moments obtained at each station. Then, based on these obtained values of the final moment, the final moment magnitudes were calculated and reported in accordance with Eq. (1). Note that, because the average radiation pattern is used in the calculations, it is ideal to have the data of an earthquake that was recorded with several stations with a good azimuthal coverage. Although some studies have shown that the radiation pattern in theory is larger than that the one observed in reality (Abercrombie 1995; Gou et al. 1992), to consider the effect of the radiation pattern in the final calculations, all earthquakes that had at least three well-recorded good quality accelerograms were selected. Therefore, for the statistical analysis, all earthquakes with reported  $M$  and at least three recorded accelerograms were first selected and then the magnitude residual values for each earthquake was calculated based on the two selected windows. Subsequently, the Mean and the  $\sigma$  of magnitude residuals were calculated. Eventually, the calculation has been done for a total of 209



**Table 3** The resulted values of seismic moment ( $M_0$ ), estimated magnitude ( $M_{cal}$ ), and corner frequency ( $f_c$ ) for 2017 Sarpol-e Zahab earthquake using accelerograms with epicentral distance less than 150 km based on W-window

Record	Station	Epicentral distance (km)	Mcal	M0 (N.m)	fc (Hz)
7384–1	Sarpolezahab	39.22	7.37	1.26E+20	0.12
7297	Nosood	47.28	6.87	2.29E+19	0.12
7377–1	Goorsefid	66.1	7.12	5.41E+19	0.18
7302–1	Kerend	66.33	7.24	8.10E+19	0.16
7310	Degaga	67.31	6.91	2.63E+19	0.11
7279	Palangan	69.5	6.92	2.65E+19	0.12
7290	Sarv Abad	69.63	6.85	2.13E+19	0.11
7287	Marivan	82.54	6.93	2.82E+19	0.16
7317	Shoeisheh	92.65	7.07	4.57E+19	0.1
7278	Kamyaran	92.97	7.01	3.65E+19	0.11
7313	Eslamabadqarb	96.33	7.38	1.33E+20	0.14
7295	Mahidasht	101.45	6.99	3.40E+19	0.26
7281	Sanandaj2	113.33	6.73	1.40E+19	0.18
7280	Sanandaj1	113.59	7	3.53E+19	0.13
7294	Homail	124.91	7.35	1.20E+20	0.09
7311	Deh Golan	146.44	7.08	4.60E+19	0.28
Mean			7.05	4.39E+19	0.15

**Table 4** Mean and standard deviation ( $\sigma$ ) values of the magnitude residuals for all records

All accelerograms	Mean residual	Standard deviation ( $\sigma$ )
W-window	0.09	0.35
S-window	0.09	0.31

earthquakes. Table 5 shows the mean residual values and the standard deviations for the earthquakes that have reported  $M$  and at least three recorded accelerograms with good quality for the selected windows. Also, part (e) of Figs. 5 and 6 shows the calculated magnitudes versus reported magnitudes along with the obtained standard deviation for these earthquakes. Based on the obtained results, it is suggested that Andrews’ method offers results that are in accordance with the reported magnitude (especially for events with  $M < 7.0$ ), mean residual values of about 0.07 and standard deviations ( $\sigma$ ) about 0.2. However,

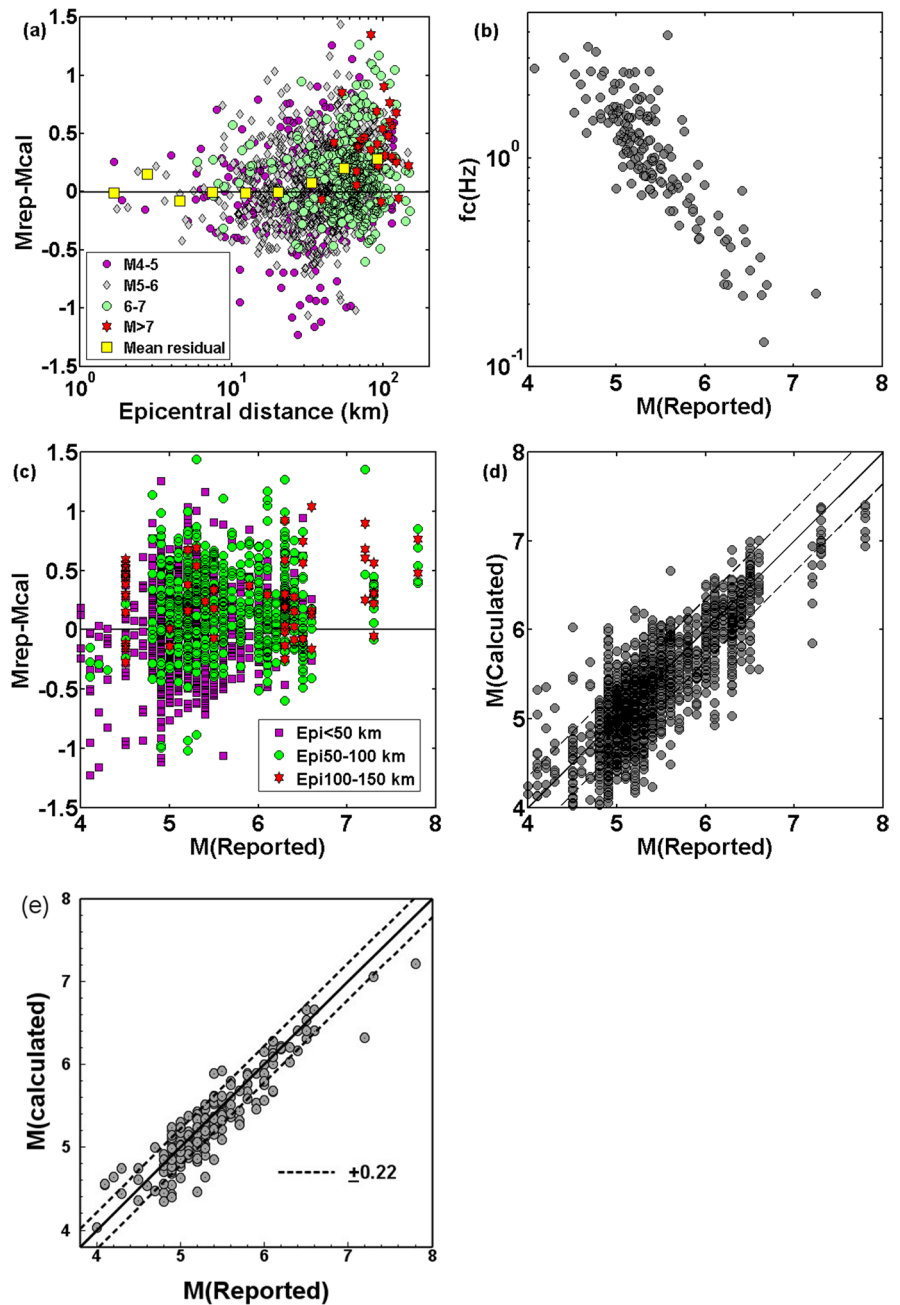
we observe larger underestimation of magnitude for earthquakes with  $M > 7.0$  in our database. The results suggest that the Andrews method with the two selected windows yields almost the same mean residuals and standard deviations. However, the S-window has a relatively lower standard deviation. Because of the 0.08 and 0.07 unit of magnitude underestimation for two selected windows, we propose to add these mean residual values to the calculated magnitude when the  $M_{cal} \geq 5.0$  is obtained since the larger magnitude earthquakes are more important in emergency response and civil protection purposes.

Corner frequency is calculated for each record and then the mean value of  $f_c$  obtained from different stations for each earthquake was calculated. Part (b) in Figs. 5 and 6 shows the obtained  $f_c$  vales versus reported magnitudes. As was foreseeable, a linear relationship between logarithm of  $f_c$  and the magnitude is observed. It is expected that larger events have smaller  $f_c$ , which is clearly demonstrated in part (b) of Figs. 5 and 6.

### 7 Discussions and conclusions

In this study, using the ISMN accelerograms, source parameters including  $M_0$ ,  $M$ , and  $f_c$  of the earthquakes were calculated. As described in the preceding sections,  $M_0$  values and  $M$  are obtained by Andrews (1986) method for the W- and S- windows, where the obtained values show a good agreement with the reported magnitudes by the international centers (for events that had reported  $M$ ). Nevertheless, we observed underestimation of the calculated magnitude for the large events ( $M > 7.0$ ) in our dataset using this method. Unfortunately, we have just three earthquakes with  $M > 7.0$  that had atleast three records, where two of them were not recorded very well. For example, the largest event in our catalogue, the  $M7.8$  earthquake on 2013/04/16 occurred in Pakistan and all of the recorded data of this earthquake have been recorded just from one side at a relatively large distance; also, the quality of some of these data is not that high. By contrast, the  $M7.3$  Sarpol-e Zahab earthquake was recorded very well by many stations across the country. The obtained magnitude for Sarpol-e Zahab earthquake is 0.2 underestimated, where this value is close to the standard deviation of the results (Table 5). However, for the other two earthquakes, we do not have very well recorded data. Not

**Fig. 5** The obtained results using the W-window: **a** residuals ( $M_{rep}-M_{cal}$ ) for all records versus the epicentral distance (km), different symbols show the magnitude range, and squares show the bin averaged residuals. **b** Corner frequency values calculated for all earthquakes with at least 3 records versus the calculated magnitudes. **c** Residuals ( $M_{rep}-M_{cal}$ ) for all accelerograms versus the reported moment magnitude ( $M$  (reported)), different symbols represent the epicentral distance range. **d** The calculated magnitude ( $M$  (calculated)) against the  $M$  (reported) for all records and the resulted standard deviation of 0.35. **e** The calculated magnitude for each earthquake against  $M$  (reported) along with the resulted standard deviation of 0.22

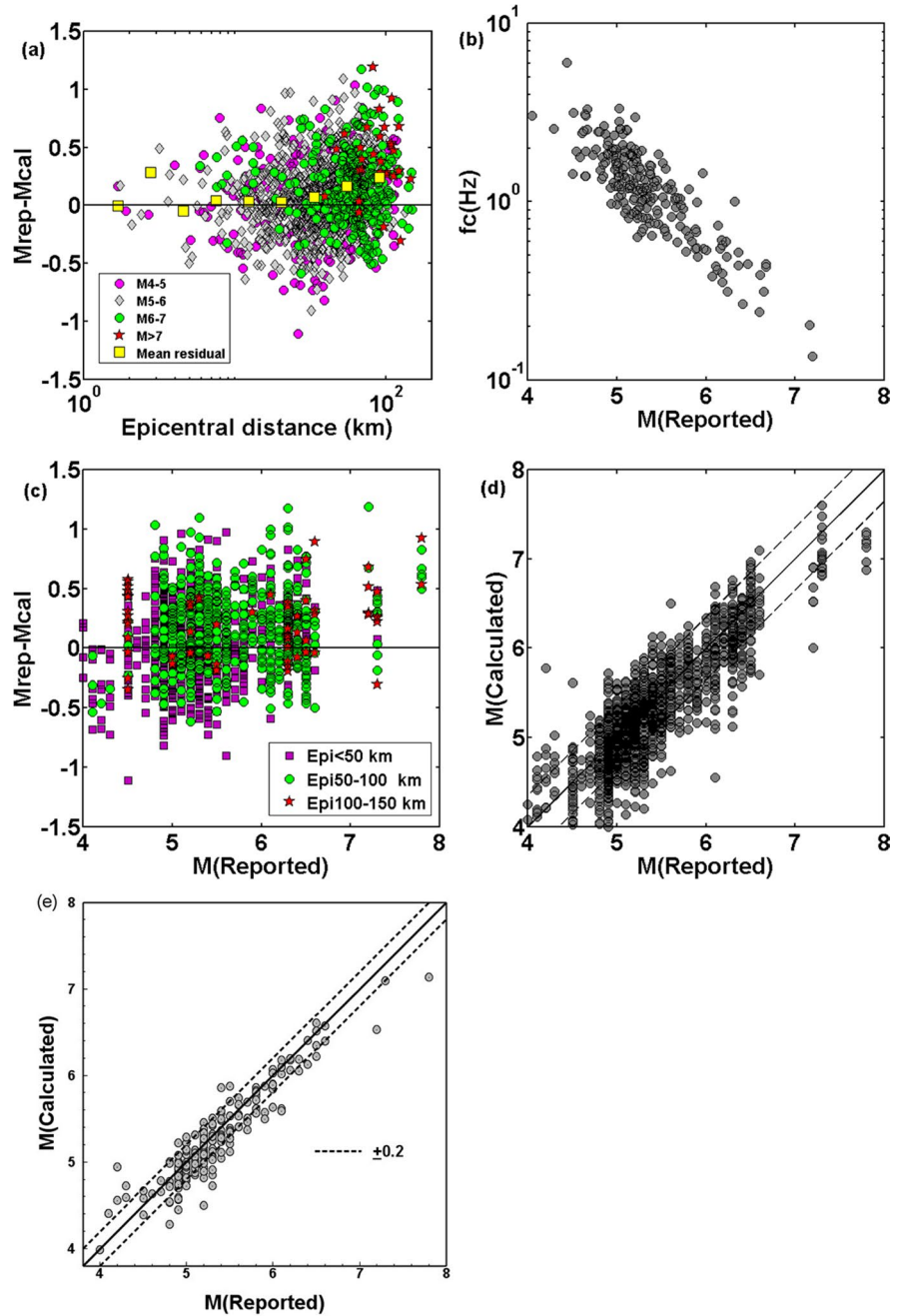


having many large earthquake in our dataset makes it difficult to judge the performance of this method for very large earthquake (i.e.,  $M > 7.0$ ).

Figures 5 and 6 (parts a, and c) reveal that overall the magnitude is underestimated in larger distance ( $R > 50$  km). One major factor could be the effect of the selected geometrical spreading model. It is well established that a trade-off exists between source

parameters and geometric attenuation (Boore et al. 2010). Potentially, other geometrical spreading functions could be chosen; however, here, we selected the simplest model that can relatively accommodate these effects. Further investigation to develop an attenuation model for Iran and verify the geometrical spreading rates over a wide range of distances is suggested.

**Fig. 6** The obtained results using the S-window: **a** residuals (Mrep-Mcal) for all records versus the epicentral distance (km), different symbols show the magnitude range, and squares show the bin averaged residuals. **b** Corner frequency values calculated for all earthquakes with at least 3 records versus the calculated magnitudes. **c** Residuals (Mrep-Mcal) for all accelerograms versus the reported moment magnitude ( $M$  (reported)), different symbols represent the epicentral distance range. **d** The calculated magnitude ( $M$  (calculated)) against the  $M$  (reported) for all records and the resulted standard deviation of 0.31. **e** The calculated magnitude for each earthquake against  $M$  (reported) along with the resulted standard deviation of 0.20



Another important fact to be considered is the filtering since we filter the data, it should be borne in mind that for very strong earthquakes ( $M \geq 7.5$ ) it is possible to lose the corner frequency information of the earthquake due to data filtering. In other words, because larger earthquakes have more energy at lower frequencies, a filter frequency higher than

corner frequency of earthquake may be selected during the data correction, and thus, information about the important part of the earthquake energy would be lost. Therefore, the magnitude will be underestimated. For example, the corner frequency of an earthquake with  $M8.3$  is about 0.03, and the magnitude of the earthquake is probably less estimated if the selected

**Table 5** The resulted mean (mean) and standard deviation ( $\sigma$ ) of the residuals for earthquake with at least 3 recorded accelerograms and reported moment magnitude. S and W represent the S- and W-window respectively

Calculated magnitude	Mean residual	Standard deviation ( $\sigma$ )
W_window	0.08	0.22
S_window	0.07	0.2

filter frequency based on the SNR is larger than 0.03. However, for most part of Iran (except Makran zone), the probability of occurrence of earthquake with  $M > 8.0$  is very unlikely.

Overall, considering the types of factors involved in the source parameters estimation, calculation of the errors in the resulted source parameter is not an easy task (Abercrombie 1995). For example, in our procedure, the site effects that has influence on the spectral amplitudes has not been taken into account. Nonetheless, it is not an easy task to consider the site effect in these type of source estimation and this would have strong effect on resulted values, especially for corner frequency that was pointed out by previous studies as well (e.g., Abercrombie 1995; Caprio et al. 2011; Gallo et al. 2014).

According to the results of this study, the use of both selected windows results in a similar standard deviation. Note that in this study, moment magnitude has been calculated and presented for a considerable number of ISMN accelerograms. Usually for small and medium size earthquakes, the  $M$  is not reported by international centers. In such cases, with the results of this study,  $M$  can be estimated independently from other references and only using the accelerograms database. In this regard, many of the available accelerograms, which for various reasons their focal mechanism or moment tensor solution are unknown, and therefore, the resultant  $M$  of the earthquake is not known either, can have an estimation of their  $M$ ; this is valuable in studies of earthquake hazard and other related researches. Also, in forward-modeling studies of seismic and strong motion record, a weak motion record is often used as a Green function for the modeling of the effects of wave propagation to the target site. In these types of modeling, the size of the network cells on the fault plane is extracted from the  $M$  of the causing earthquake. Usually, for such weak

recordings, the  $M$  is not known, which is now calculable with the above explanation.

Another notable point is the fact that, the magnitude obtained from this method is much faster than conventional methods based on the seismic data, which can be very useful in the application of earthquake early warning (EEW) and rapid response systems as well as in the crisis management. Another remarkable point is that the data with smaller distances to the source provide more precise results at a shorter time. In the EEW and rapid response systems, these values play a vital role. With the precise value of the seismic source parameters as well as the earthquake strong motion parameters, we are able to provide an EEW with less error, and more accurate shake maps, resulting in a better and more effective earthquake response. As a result, installing high-quality accelerometers in seismically active areas of the country that have the capability to record the high quality earthquake strong motion in the near field can be very helpful in reducing and managing the earthquake hazards. Therefore, updating and modernizing of the available accelerometers, as well as installing the new modern instruments, are very helpful to reduce earthquake casualties and earthquake damage along with better crises management after an earthquake.

**Acknowledgements** We acknowledge the Plan and Budget organization and Ministry of Road and Housing for supporting the Iran Strong Motion project and providing the access to the strong motion data for scientist, students, and researchers. We also would like to appreciate two anonymous reviewers for their useful remarks and suggestions that have contributed to improve the manuscript.

**Data availability** All strong motion records selected in this study were obtained from Iran Strong Motion Network (ISMN; <https://doi.org/10.7914/SN/I1>). Data can be obtained from ISMN portal at <https://ismn.bhrc.ac.ir/> (last accessed June 2018). The Global Centroid Moment Tensor Project database was accessed using [www.globalcmt.org/CMTsearch.html](http://www.globalcmt.org/CMTsearch.html) (last accessed on June 2018). Moment magnitude information from National Earthquake Information Center was searched using <https://earthquake.usgs.gov/earthquakes/search/> (last accessed on June 2018). The information from Iran Seismological Center was obtained from <http://irsc.ut.ac.ir/focal.php> (last accessed on July 2018).

#### Declarations

**Conflict of interest** The authors declare no competing interests.

## References

- Aki K (1966) Generation and propagation of G waves from the Niigata earthquake of June 14, 1964. Part 2. Estimation of earthquake moment, released energy and stress-strain drop from G wave spectrum. *Bull Earthq Res Inst* 44:73–88
- Aki K (1972) Earthquake mechanism. *Tectonophysics* 13:423–441
- Aki K, Richards PG (1980) *Quantitative seismology*. W.H Freeman, San Francisco, California, p 932
- Andrews DJ (1986) Objective determination of source parameters and similarity of earthquakes of different size. *Maurice Ewing series, 6, American Geophysical Union, Geophysics Monograph, 37, Washington DC, 259–267*
- Boatwright J (1980) A spectral theory for circular seismic sources; simple estimates of source dimension, dynamic stress drop, and radiated seismic energy. *Bull Seismol Soc Am* 70:1–27
- Bommer JJ, Pereira AM (1999) The effective duration of earthquake strong motion. *J Earthq Eng* 3(2):127–172
- Boore D (1983) Stochastic simulation of high-frequency ground motions based on seismological models of the radiated spectra. *Bull Seismol Soc Am* 73(6):1865–1894
- Boore DM, Boatwright J (1984) Average body-wave radiation coefficients. *Bull Seism Soc Am* 74:1615–1621
- Boore DM, Campbell KW, Atkinson GM (2010) Determination of stress parameters for eight well-recorded earthquakes in eastern North America. *Bull Seism Soc Am* 100:1632–1645
- Brune JN (1970) Tectonics stress and the spectra of seismic shear waves from earthquakes. *J Geophys Res* 75:4997–5009
- Brune JN (1971) Correction. *J Geophys Res* 76:4997–5009
- Caprio M, Lancieri M, Cua GB, Zollo A, Wiemer S (2011) An evolutionary approach to real-time moment magnitude estimation via inversion of displacement spectra. *Geophys Res Lett* 38:L02301. <https://doi.org/10.1029/2010GL045403>
- Chin B, Aki K (1991) Simultaneous study of the source, path, and site effects on strong ground motion during the 1989 Loma Prieta Earthquake: a preliminary result on pervasive nonlinear site effects. *Bull Seism Soc Am* 81:1859–1884.
- Davatgari FTM, Singh Bora S, Mirzaei N, Ghofrani H, Kazemian J (2021) Spectral models for seismological source parameters, path attenuation and site-effects in Alborz region of northern Iran. *Geophys J Int* 227:350–367. <https://doi.org/10.1093/gji/ggab227>
- Di Bona M, Rovelli A (1988) Effects of the bandwidth limitation on stress drops estimated from integrals of the ground motion. *Bull Seismol Soc Am* 78(5):1818–1825
- Edward B, Allmann B, Fäh D, Clinton J (2010) Automatic computation of moment magnitudes for small earthquakes and the scaling of local to moment magnitude. *J Geophys Res* 115:407–420
- Gallo A, Costa G, Suhadolc P (2014) Near real-time automatic moment magnitude estimation. *Bull Earthquake Eng* 12:185–202. <https://doi.org/10.1007/s10518-013-9565-x>
- Gou HA, lerner-Lam A, Hough SE (1992) Empirical Green's function study of Loma Prieta aftershocks: evidence for fault zone complexity (abstract). *Seimol Res Lett* 63:76
- Hanks TC, Kanamori H (1979) A moment magnitude scale. *J Geophys Res* 84:2348–2350. <https://doi.org/10.1029/JB084iB05p02348>
- Herrmann RB, Kijko A (1983) Modeling some empirical vertical component Lg relations. *Bull Seism Soc Am* 73:157–171
- Hwang RD, Wang JH, Huang BS, Chen KC, Huang WG, Chang TM, Chiu HC, Tsai CP (2001) Estimates of stress drop of the Chi-Chi, Taiwan, Earthquake of 20 September 1999 from near-field seismograms. *Bull Seism Soc Am* 91:1158–1166
- Kanamori H (1977) The energy release in great earthquakes. *J Geophys Res* 82:1981–1987
- Kanamori H (1983) Magnitude scale and quantification of earthquakes. *Tectonophysics* 93:185–199
- Kikuchi M, Kanamori H (1991) Inversion of complex body waves—III. *Bull Seism Soc Am* 81:2335–2350
- Parolai D, Bindi D, Durukal E, Grosser H, Milkereit C (2007) Source parameters and seismic moment-magnitude scaling for northwestern Turkey. *Bull Seism Soc Am* 97(2):655–660. <https://doi.org/10.1785/0120060180>
- Richter CF (1935) An instrumental earthquake magnitude scale. *Bull Seism Soc Am* 25:1–32
- Shahvar M, Zare M, Castellaro S (2013) A unified seismic catalog for the Iranian Plateau (1900–2011). *Seismol Res Lett* 84(2):233–249. <https://doi.org/10.1785/0220120144>
- Shahvar M, Farzanegan E, Eshaghi A, Mirzaei H (2021) i1-net: the Iran Strong Motion Network. *Seismo Res Lett* 92(4):2100–2108. <https://doi.org/10.1785/0220200417>
- Shoja-Taheri J, Naserieh D, Ghofrani H (2007) ML and MW scales in the Iranian plateau based on the strong-motion records. *Bull Seism Soc Am* 97(2):661–669. <https://doi.org/10.1785/0120060132>

**Publisher's Note** Springer Nature remains neutral with regard to jurisdictional claims in published maps and institutional affiliations.

Springer Nature or its licensor holds exclusive rights to this article under a publishing agreement with the author(s) or other rightsholder(s); author self-archiving of the accepted manuscript version of this article is solely governed by the terms of such publishing agreement and applicable law.